

Simultaneous UV Images and High-Latitude Particle and Field Measurements During an Auroral Dawn Storm at Jupiter

R. W. Ebert, T. K. Greathouse, G. Clark, V. Hue, F. Allegrini, F. Bagenal, S. J. Bolton, B. Bonfond, J. E. P. Connerney, G. R. Gladstone, et al.

▶ **To cite this version:**

R. W. Ebert, T. K. Greathouse, G. Clark, V. Hue, F. Allegrini, et al.. Simultaneous UV Images and High-Latitude Particle and Field Measurements During an Auroral Dawn Storm at Jupiter. Journal of Geophysical Research Space Physics, 2021, 126, 10.1029/2021JA029679 . insu-03672338

HAL Id: insu-03672338

https://insu.hal.science/insu-03672338

Submitted on 9 Dec 2022

HAL is a multi-disciplinary open access archive for the deposit and dissemination of scientific research documents, whether they are published or not. The documents may come from teaching and research institutions in France or abroad, or from public or private research centers.

L'archive ouverte pluridisciplinaire **HAL**, est destinée au dépôt et à la diffusion de documents scientifiques de niveau recherche, publiés ou non, émanant des établissements d'enseignement et de recherche français ou étrangers, des laboratoires publics ou privés.

Copyright

Check for updates

JGR Space Physics

RESEARCH ARTICLE
10.1029/2021JA029679

Key Points:

- Juno concurrently observed UV emissions from a Jupiter dawn storm and high-latitude plasma mapping to them at radial distances of ~6–8 R_J
- Electron distributions with energies from ~10 to 1,000 keV carried a significant fraction of the energy flux needed to produce the UV emissions
- Energetic ions, magnetic perturbations, whistler mode waves, and bKOM radio emissions were observed on field lines mapping to the dawn storm

Correspondence to:
R. W. Ebert,
rebert@swri.edu

Citation:
Ebert, R. W., Greathouse, T. K., Clark, G., Hue, V., Allegrini, F., Bagenal, F., et al. (2021). Simultaneous UV images and high-latitude particle and field measurements during an auroral dawn storm at Jupiter. *Journal of Geophysical Research: Space Physics*, *126*, e2021JA029679. https://doi.org/10.1029/2021JA029679

Received 15 JUN 2021
Accepted 3 NOV 2021

Author Contributions:

Conceptualization: R. W. Ebert, T. K. Greathouse, B. Bonfond, M. F. Thomsen
Data curation: R. W. Ebert, T. K. Greathouse, G. Clark, V. Hue, J. E. P. Connerney, G. R. Gladstone, W. S. Kurth, P. Louarn, B. H. Mauk, C. Paranicas, A. H. Sulaiman
Formal analysis: R. W. Ebert, T. K. Greathouse, G. Clark, V. Hue, F. Allegrini, S. Kotsiaros, A. H. Sulaiman, J. R. Szalay
Funding acquisition: S. J. Bolton
Investigation: R. W. Ebert, T. K. Greathouse
Methodology: R. W. Ebert, T. K. Greathouse, G. Clark
Project Administration: R. W. Ebert
Resources: R. W. Ebert
Software: R. W. Ebert, T. K. Greathouse, R. J. Wilson
Validation: R. W. Ebert

© 2021. American Geophysical Union. All Rights Reserved.

Simultaneous UV Images and High-Latitude Particle and Field Measurements During an Auroral Dawn Storm at Jupiter

R. W. Ebert[1,2], T. K. Greathouse[1], G. Clark[3], V. Hue[1], F. Allegrini[1,2], F. Bagenal[4], S. J. Bolton[1], B. Bonfond[5], J. E. P. Connerney[6,7], G. R. Gladstone[1,2], M. Imai[8], S. Kotsiaros[9], W. S. Kurth[10], S. Levin[11], P. Louarn[12], B. H. Mauk[3], D. J. McComas[13], C. Paranicas[3], A. H. Sulaiman[10], J. R. Szalay[13], M. F. Thomsen[14], and R. J. Wilson[4]

[1]Southwest Research Institute, San Antonio, TX, USA, [2]Department of Physics and Astronomy, University of Texas at San Antonio, San Antonio, TX, USA, [3]Johns Hopkins University Applied Physics Lab, Laurel, MD, USA, [4]Laboratory for Atmospheric and Space Physics, University of Colorado Boulder, Boulder, CO, USA, [5]Université de Liège, Liège, Belgium, [6]Space Research Corporation, Annapolis, MD, USA, [7]NASA Goddard Space Flight Center, Greenbelt, MD, USA, [8]Department of Electrical Engineering and Information Science, National Institute of Technology, Niihama College, Niihama, Japan, [9]DTU Space, Technical University of Denmark, Kgs. Lyngby, Denmark, [10]Department of Physics and Astronomy, University of Iowa, Iowa City, IA, USA, [11]Jet Propulsion Laboratory, Pasadena, CA, USA, [12]Institut de Recherche en Astrophysique et Planétologie, Toulouse, France, [13]Department of Astrophysical Sciences, Princeton University, Princeton, NJ, USA, [14]Planetary Science Institute, Tucson, AZ, USA

Abstract We present multi-instrument Juno observations on day-of-year 86, 2017 that link particles and fields in Jupiter's polar magnetosphere to transient UV emissions in Jupiter's northern auroral region known as *dawn storms*. Juno ranged from 42°N to 51°N in magnetic latitude and 5.8–7.8 Jovian radii (1 R_J = 71,492 km) during this period. These dawn storm emissions consisted of two separate, elongated structures which extended into the nightside, rotated with the planet, had enhanced brightness (up to at least 1.4 megaRayleigh) and high color ratios. The color ratio is a proxy for the atmospheric penetration depth and therefore the energy of the electrons that produce the UV emissions. Juno observed electrons and ions on magnetic field lines mapping to these emissions. The electrons were primarily field-aligned, bidirectional, and, at times, exhibited sudden intensity decreases below ~10 keV coincident with intensity enhancements up to energies of ~1,000 keV, consistent with the high color ratio observations. The more energetic electron distributions had characteristic energies of ~160–280 keV and downward energy fluxes (~70–135 mW m^{-2}) that were a significant fraction needed to produce the UV emissions for this event. Magnetic field perturbations up to ~0.7% of the local magnetic field showing evidence of upward and downward field-aligned currents, whistler mode waves, and broadband kilometric radio emissions were also observed along Juno's trajectory during this time frame. These high-latitude observations show similarities to those in the equatorial magnetosphere associated with dynamics processes such as interchange events, plasma injections, and/or tail reconnection.

1. Introduction

The primary components of Jupiter's ultraviolet (UV) aurora are the main, outer, polar, and satellite emissions (see review by Grodent et al., 2015 for details). These emissions are produced primarily by precipitating electrons interacting with H_2 molecules in Jupiter's upper atmosphere (e.g., Broadfoot et al., 1979) and can be used as a diagnostic of dynamics and structure in Jupiter's magnetosphere. A number of secondary, transient UV auroral emissions have also been identified, many occurring in the dawn sector of Jupiter's auroral region (e.g., Ballester et al., 1996; Bonfond et al., 2021; Clarke et al., 1998; Gérard et al., 1994; Gustin et al., 2006; Kimura et al., 2015, 2017; Prangé et al., 1993; Radioti et al., 2008; Yao et al., 2020).

Using UV images from the Faint Object Camera on the Hubble Space Telescope (HST), Gérard et al. (1994) identified a bright, arc-like UV feature of ~6 megaRayleigh (MR) in Jupiter's northern auroral region that was in quasi-corotation with the planet. This feature dimmed by more than an order of magnitude when it was observed again ~20 hr later, suggesting a transient phenomenon that was attributed to large-scale

21699402, 2021, 12, Downloaded from https://agupubs.onlinelibrary.wiley.com/doi/10.1029/2021JA029679 by Portail BibCNRS INSU, Wiley Online Library on [09/12/2022]. See the Terms and Conditions (https://onlinelibrary.wiley.com/terms-and-conditions) on Wiley Online Library for rules of use; OA articles are governed by the applicable Creative Commons License

Visualization: R. W. Ebert, T. K. Greathouse, V. Hue
Writing – original draft: R. W. Ebert
Writing – review & editing: R. W. Ebert, T. K. Greathouse, G. Clark, V. Hue, F. Allegrini, F. Bagenal, B. Bonfond, J. E. P. Connerney, S. Kotsiaros, W. S. Kurth, P. Louarn, B. H. Mauk, D. J. McComas, C. Paranicas, A. H. Sulaiman, J. R. Szalay, M. F. Thomsen, R. J. Wilson

variations in Jupiter's magnetospheric current system. Clarke et al. (1998) identified bright, transient UV emissions in the local dawn region near the expected location of Jupiter's main emission. These emissions, coined "dawn storms," showed significant spreading in longitude and remained near local dawn while other, dimmer, emissions corotated with the planet. Their proximity to the main aurora suggested that these emissions were produced in Jupiter's middle magnetosphere. Kimura et al. (2015) interpreted these dawn storms as being driven by tail reconnection, bringing energetic particles from the outer and middle magnetosphere to the inner magnetosphere within a time frame of up to 2 planetary rotations. Gustin et al. (2006) reported on dawn UV auroral brightenings of up to ∼1.8 MR, ∼4 times brighter than the nominal main emission (Grodent et al., 2003). These features had a leading edge that was fixed in system III longitude (a system fixed with the corotating planet) whereas the trailing edge seemed to be organized by local time, with an extension into the nightside of Jupiter's auroral region. UV spectral observations were used to infer the characteristic energies (up to ∼50–500 keV), energy fluxes (5–90 mW m^{-2}), and current densities (∼0.1–0.5 μA m^{-2}) of the precipitating electrons responsible for producing these emissions (Gustin et al., 2006). These electrons were interpreted as being accelerated by electric fields in regions of upward field-aligned currents.

In July 2016, NASA's Juno mission (Bolton et al., 2017) was inserted into a 53-day polar orbit around Jupiter. Juno is a spinning spacecraft with a ∼30-s spin period. Its orbit and suite of instruments provide an excellent platform to remotely image Jupiter's aurora (e.g., Connerney, Adriani, et al., 2017) while simultaneously measuring in situ the polar magnetospheric environment that map to unique auroral emissions (e.g., Ebert et al., 2019; Gérard et al., 2019). The Juno observations present a new opportunity to study the physics of dawn storms at Jupiter. For instance, Bonfond et al. (2021) examined the complete process of dawn storm evolution using global images of these events provided by Juno along with their frequency. They found that dawn storms originate as small, short-lived emissions followed a couple of hours later by the evolution from a linear to a more irregular arc in the main emission in the midnight region which then rotates toward dawn. After broadening and then splitting, these emissions are separated by a region absent of emissions that fills in as the event progresses. The final stage produces equatorward-moving auroral emissions associated with plasma injection signatures. Considered as a sequence, these auroral features were interpreted as the signature of magnetotail reconfigurations, including reconnection, plasma instabilities, dipolarization, and plasma injections. They also determined that dawn storms are present in approximately half of the 8-hr long perijove sequences during Juno's first 20 perijoves.

Yao et al. (2020) combined in-situ particle and field measurements in Jupiter's equatorial magnetosphere from Juno with auroral observations from the HST. They found that auroral dawn storm emissions were often observed in conjunction with auroral signatures attributed to particle injections in the equatorial magnetosphere. They suggested that the drivers of these emissions may be physically connected, with magnetic reconnection in the dawn side magnetosphere being responsible for the auroral dawn storms and the subsequent magnetic dipolarization producing the auroral injection signatures. Swithenbank-Harris et al. (2021) also examined in-situ measurements from Juno in Jupiter's equatorial dawn magnetosphere concurrent with an auroral dawn storm observed by HST. Their analysis revealed a source region located at ∼60 R_J with a component rotating toward local noon and proton velocities to near corotation speeds. The source region was characterized by enhanced densities of hot plasma, field-aligned energetic protons, and heavy ions, and a reversal in the azimuthal component of Jupiter's magnetic field. They suggested that dawn storms result from the acceleration and heating of magnetospheric plasma following reconnection at earlier local times.

In this study, we present UV images and in-situ particle and field observations in Jupiter's polar magnetosphere associated with a dawn storm in Jupiter's northern auroral region on day-of-year (DOY) 86, 2017, prior to Juno's 5th perijove (PJ5). We focus on the period from 03:00 to 05:00 UT when Juno ranged from 7.8 R_J to 5.8 R_J in jovicentric radial distance and 41.6°N to 50.9°N in magnetic latitude. This period is of high interest because the spacecraft simultaneously imaged the UV emissions it was magnetically connected to. This was the first time that Juno was at high latitude and on magnetic field lines connecting to a dawn storm. Section 2 provides an overview of the Juno data sets and observing geometry used in this study. UV brightness and color ratio images and polar magnetosphere particle and field observations are presented in Section 3. Section 4 provides an interpretation of the observations. A summary and conclusions are

21699402, 2021, 12, Downloaded from https://agupubs.onlinelibrary.wiley.com/doi/10.1029/2021JA029679 by Portail BibCNRS INSU, Wiley Online Library on [09/12/2022]. See the Terms and Conditions (https://onlinelibrary.wiley.com/terms-and-conditions) on Wiley Online Library for rules of use; OA articles are governed by the applicable Creative Commons License

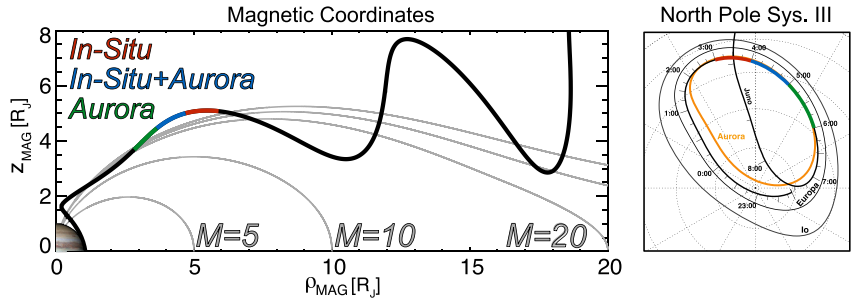


Figure 1. (left) Juno's inbound trajectory (black line) in Jupiter's northern hemisphere prior to perijove 5 on days-of-year 85–86, 2017. The trajectory is shown in a magnetic coordinate system (Connerney et al., 1981, 2018). Magnetic field lines, and the M-shells that they map to, are shown in gray. (right) Magnetic projection of Juno's trajectory onto the 1-bar level of Jupiter's upper atmosphere in black with times indicated. Orange oval denotes the statistical average position of Jupiter's main ultraviolet aurora (Bonfond et al., 2012). Thick red, blue, and green lines highlight the periods of interest along Juno's trajectory. Dashed circles and lines are contours of constant jovicentric latitude and system III longitude, respectively. Black ovals identify the location of the Io (outer) and Europa (inner) auroral footprint paths.

presented in Section 5. These Juno observations provide a unique opportunity to study particle and field features at high latitude that directly map to transient UV emissions observed in Jupiter's dawn auroral region.

2. Data Sets and Observing Geometry

We examine electron and ion observations from Juno's Jovian Auroral Distributions Experiment Electron (JADE-E) and Ion (JADE-I) sensors (McComas et al., 2017) and Jupiter Energetic particle Detector Instrument (JEDI) (Mauk, Haggerty, et al., 2017), UV emissions from Juno's ultraviolet spectrograph (UVS) (Gladstone et al., 2017), radio and plasma wave observations from the Waves instrument (Kurth et al., 2017), and magnetic field observations from the Magnetic Field Investigation (MAG) (Connerney, Benn, et al., 2017). JADE-E and JEDI measure electron fluxes in the energy range of 0.1–100 and 30–1,000 keV, respectively, along with their pitch angle distributions, with a time resolution up to 1 s. JADE-I measures ions from 0.01 to 46 keV/charge (keV/q) over a mass per charge (m/q) range of ~1–64 amu at a time resolution as high as 2 s. JEDI measures ions with total energy from ~50 keV to well above 1 MeV (upper limit is species dependent), along with their pitch angle distributions and can resolve oxygen and sulfur above ~400 keV. UVS is an imaging spectrograph sensitive to wavelengths between 68 and 210 nm. It observes Jupiter's northern and southern auroras for several hours bounding each Juno perijove pass from jovicentric distances of ~1.3–7 R_J. A scan mirror allows shifting the field-of-view (FOV) of UVS by up to ±30° above or below the spacecraft spin plane. The combination of Juno's spinning nature and UVS's scan mirror gives this instrument access to half the sky for any given spacecraft orientation. The UV brightness is determined by integrating the emissions between 155 and 162 nm and then multiplying by 8.1 to estimate the total H_2 emission between 75 and 198 nm (Gérard et al., 2019). Waves measures the wave magnetic and electric fields covering frequency ranges of 50 Hz–20 kHz and 50 Hz–40 MHz, respectively, at a time resolution of up to 1 s near Juno's perijove. MAG consists of two independent sensor suites, each containing a triaxial fluxgate magnetometer (FGM) and a pair of imaging sensors. The FGMs simultaneously measure the magnetic field at a rate of 64 vector samples per second. We utilize 1 s magnetic field vector observations from MAG to calculate the electron pitch angle distributions. See the instrument papers cited above for more details.

Figure 1 shows Juno's trajectory on approach to PJ5 and its projection onto the planet using the JRM09 internal magnetic field model (Connerney et al., 2018) and the magnetodisc model of Connerney et al. (1981), where Z_{MAG} is along Jupiter's magnetic dipole axis and ρ_{MAG} is the perpendicular distance from the magnetic dipole axis. M, or M-shell, corresponds to a distance based on the predicted magnetic equator crossing distance for any given magnetic field line. Juno's magnetic footpoint maps along Jupiter's northern main auroral oval from ~02:00 to 06:30 UT on DOY 86, 2017. The periods of interest are highlighted by the thick red, blue, and green lines. The blue line corresponds to an interval when Juno made in-situ measurements of particles, and fields while simultaneously observing bright UV features near Jupiter's main emission. The red line identifies a period when Juno made in situ measurements on field lines mapping to the expected

21699402, 2021, 12, Downloaded from https://agupubs.onlinelibrary.wiley.com/doi/10.1029/2021JA029679 by Portail BibCNRS INSU, Wiley Online Library on [09/12/2022]. See the Terms and Conditions (https://onlinelibrary.wiley.com/terms-and-conditions) on Wiley Online Library for rules of use; OA articles are governed by the applicable Creative Commons License

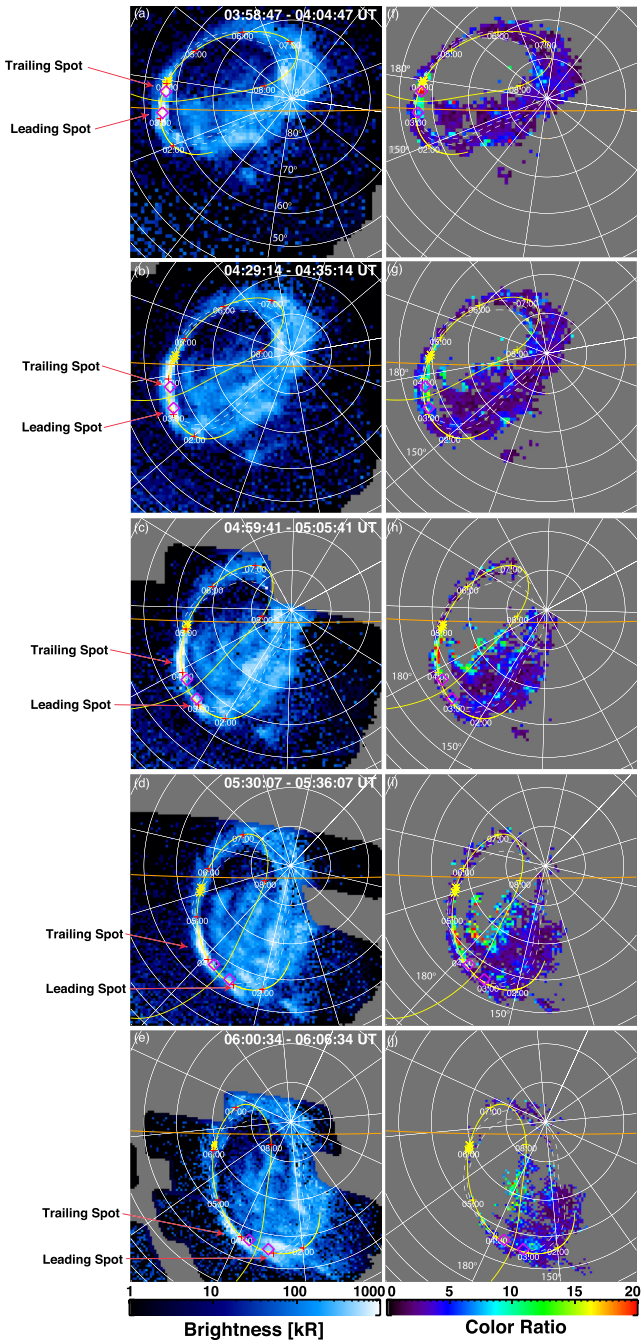


Figure 2. (a–e) Polar projections of ultraviolet (UV) brightness images in Jupiter's northern auroral region on day-of-year 86, 2017 from 03:58 to 06:06 UT. (f–j) Color ratio images for the same intervals as shown for the UV brightness. These images are in chronological order. Red arrows in (a–e) point to the emissions studied here. Yellow lines identify Juno's trajectory, the yellow stars identify Juno's footprint at the time when the UV images were collected. The purple diamonds in each panel bound the latitude and longitude for the UV emissions whose brightness and color ratio estimates are shown in Figure 3. Orange lines denote the day-night terminator, the Sun direction being the bottom of each image. The two white dashed lines represent the statistical average compressed and expanded position of Jupiter's main ultraviolet (UV) aurora (Bonfond et al., 2012).

location of the bright UV features under consideration here. The green line highlights when Juno was only remotely observing the bright UV auroral features.

3. UV Aurora and High-Latitude Magnetosphere Observations

Figure 2 presents UV brightness (left column) and color ratio (right column) maps of Jupiter's northern auroral region covering the period from 03:58 to 06:06 UT on DOY 86, 2017. Each map is a composite of 12 different images obtained over a ~6-min interval, each image having ~17 ms of integration time. The color ratio, defined as the ratio between the integrated brightness from 158 to 162 and 126 to 130 nm, is used to estimate the depth from which the UV emissions are generated and are a proxy for the characteristic energy of the precipitating electrons that produce them. A larger color ratio is interpreted as representing more energetic electrons that produce the UV emissions (e.g., Gérard & Singh, 1982), with more energetic electrons penetrating deeper into the atmosphere (e.g., Gérard et al., 2014).

This study focuses on the bright UV emissions observed on the left side of Figure 2a, near the statistical average latitude of the main aurora, denoted by the white dashed ovals (Bonfond et al., 2012). These UV emissions consist of two bright, elongated features on the dawn side of the auroral region, a leading spot near the terminator, and a trailing spot on the nightside. Figures 2a–2e are a time series of the auroral images and show that these features travel in the direction of planetary rotation. The purple diamond symbols in Figure 2 identify emissions that are tracked throughout this interval, at a system III latitude and longitude of 55.6° and 165.3°, respectively, for the leading spot and 56.8° and 174.8°, respectively, for the trailing spot (see Figure 3).

The image in Figure 2f indicates that the UV features under consideration have relatively high color ratios compared to the surrounding emissions. The color ratio for the nightside emission is greater than that for the emission near the terminator, suggesting that the nightside emissions are produced by more energetic electrons. Figures 2f–2i show that the color ratio for the trailing spot remains relatively higher than the leading spot throughout most of the interval.

Figure 3 shows a time series of the maximum brightness and color ratio for the UV emissions at the latitudes and longitudes specified within the purple diamond symbols in Figure 2, along with their uncertainties. We present a value from each image shown in Figure 2. The maximum brightness at the locations specified for the leading and trailing spots were 1,170 ± 290 kiloRayleighs (kR) and 1,380 ± 300 kR, respectively, at the beginning of the interval and 660 ± 240 kR and 100 ± 100 kR, respectively, at the end of the interval. The maximum color ratio for the leading spot ranged between 5.7 and 8.5 within the region of interest. The maximum color ratio within the trailing spot at the beginning of the interval was significantly higher compared to the leading spot and remained relatively enhanced except for the last image. This indicates that electrons producing the trailing spot were more energetic than those producing the

21699402, 2021, 12, Downloaded from https://agupubs.onlinelibrary.wiley.com/doi/10.1029/2021JA029679 by Portail BibCNRS INSU, Wiley Online Library on [09/12/2022]. See the Terms and Conditions (https://onlinelibrary.wiley.com/terms-and-conditions) on Wiley Online Library for rules of use; OA articles are governed by the applicable Creative Commons License

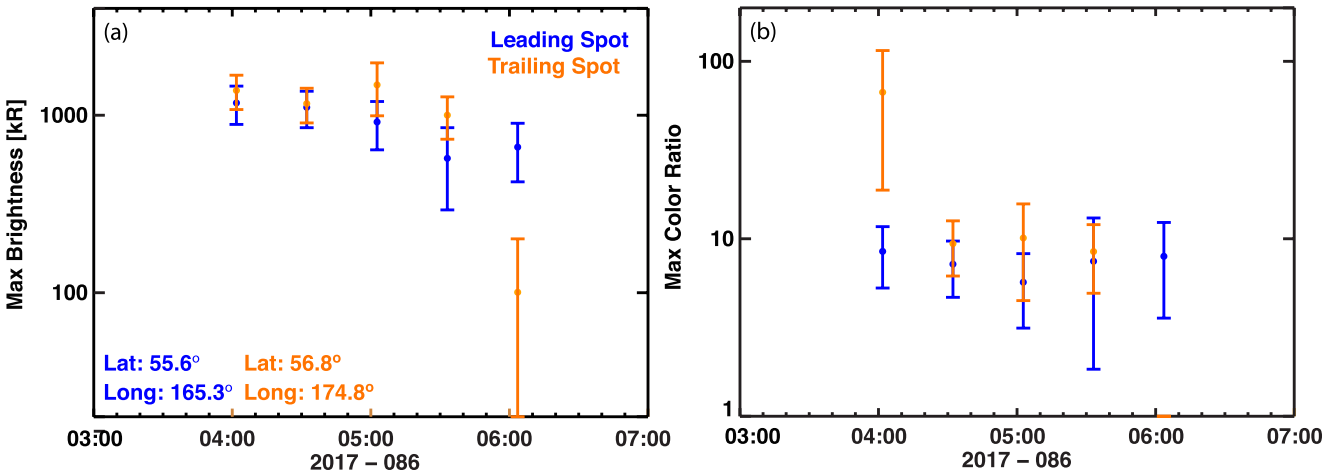


Figure 3. (a) Maximum (max) ultraviolet (UV) brightness and (b) max color ratio at latitudes and longitudes within the regions bound by the purple diamond symbols in Figure 2.

leading spot. The brightness and color ratio within both the leading and trailing spots showed a reduction in magnitude as the dawn storm progressed.

Figure 4 presents UV aurora and polar magnetosphere electron, ion, and magnetic field observations from DOY 86, 2017. The UV brightness (Figure 4a) and color ratio (Figure 4b) images were obtained from observations collected between 03:58 and 04:04 UT, a period when Juno's magnetic footprint mapped to near the trailing spot auroral features highlighted in the purple boxes. The magnetospheric observations (Figures 4c–4i) cover the time range from 03:00 to 05:00 UT. During this time frame, Juno moved toward Jupiter from 7.8 to 5.8 R_J and to higher northern magnetic latitudes from 42°N to 51°N, and its magnetic footprint mapped near the predicted location of the main emission and the bright UV emissions highlighted in Figure 2. The vertical purple rectangular box highlights particle and field observations that coincide with the timing of the auroral observations in Figures 4a and 4b.

Figure 4c shows an energy versus time spectrogram of differential energy flux for 0.1–1,000 keV electrons based on combined JEDI and JADE-E observations. The JEDI observations (>100 keV) have a 30-s time resolution throughout this period while the JADE-E observations have a resolution of 1 s from 03:00 to 03:30 UT and a 30-s resolution from 03:30 to 05:00 UT. The transition between the JADE and JEDI data presented here is at 100 keV.

The electron distributions show variations in both differential energy flux and energy. The most notable features are the depletions in low-energy electrons observed between ~03:11–03:12, 03:18–03:26, and 03:53–04:25 UT. During these times, the minimum energy of the electrons increases from <~200 eV to ≥10 keV, the bulk of their differential energy flux distributions being at energies >100 keV, with their maximum energy exceeding 500 keV. A closer inspection of the JEDI data from ~03:18 to 03:26 and 04:00 to 04:15 UT shows an enhanced electron flux just above 160 keV in the electron energy spectrogram. This signature is consistent with the presence of penetrating (>~1 MeV) electrons. The interval between 03:53 and 04:25 UT contains the period where the electrons map to near the dawn UV emissions highlighted in Figures 4a and 4b, the increase in electron energy being consistent with the high UV color ratio observations.

The pitch angle distributions for the ~30 keV–1 MeV electrons in Figure 4d are primarily between 0–30° and 150–180°, indicating that the electrons are mostly field-aligned and bidirectional at Juno's location, traveling both toward (downward) and away from (upward) Jupiter. The pitch angles for the 0.1–100 keV electrons in Figure 4e are also primarily field-aligned and bidirectional, both during times when the low-energy electrons are prominent and when they are depleted. The loss cone at Juno's radial distance during this time frame ranged from ~2.5° to 4°, which is below the pitch angle resolution for JEDI and JADE.

The 45–1,000 keV proton and 0.01–46 keV/q ion differential energy flux distributions in Figures 4f and 4g, respectively, display similar features as the electrons. Depletions in the low-energy ions are observed during

21699402, 2021, 12, Downloaded from https://agupubs.onlinelibrary.wiley.com/doi/10.1029/2021JA029679 by Portail BibCNRS INSU, Wiley Online Library on [09/12/2022]. See the Terms and Conditions (https://onlinelibrary.wiley.com/terms-and-conditions) on Wiley Online Library for rules of use; OA articles are governed by the applicable Creative Commons License

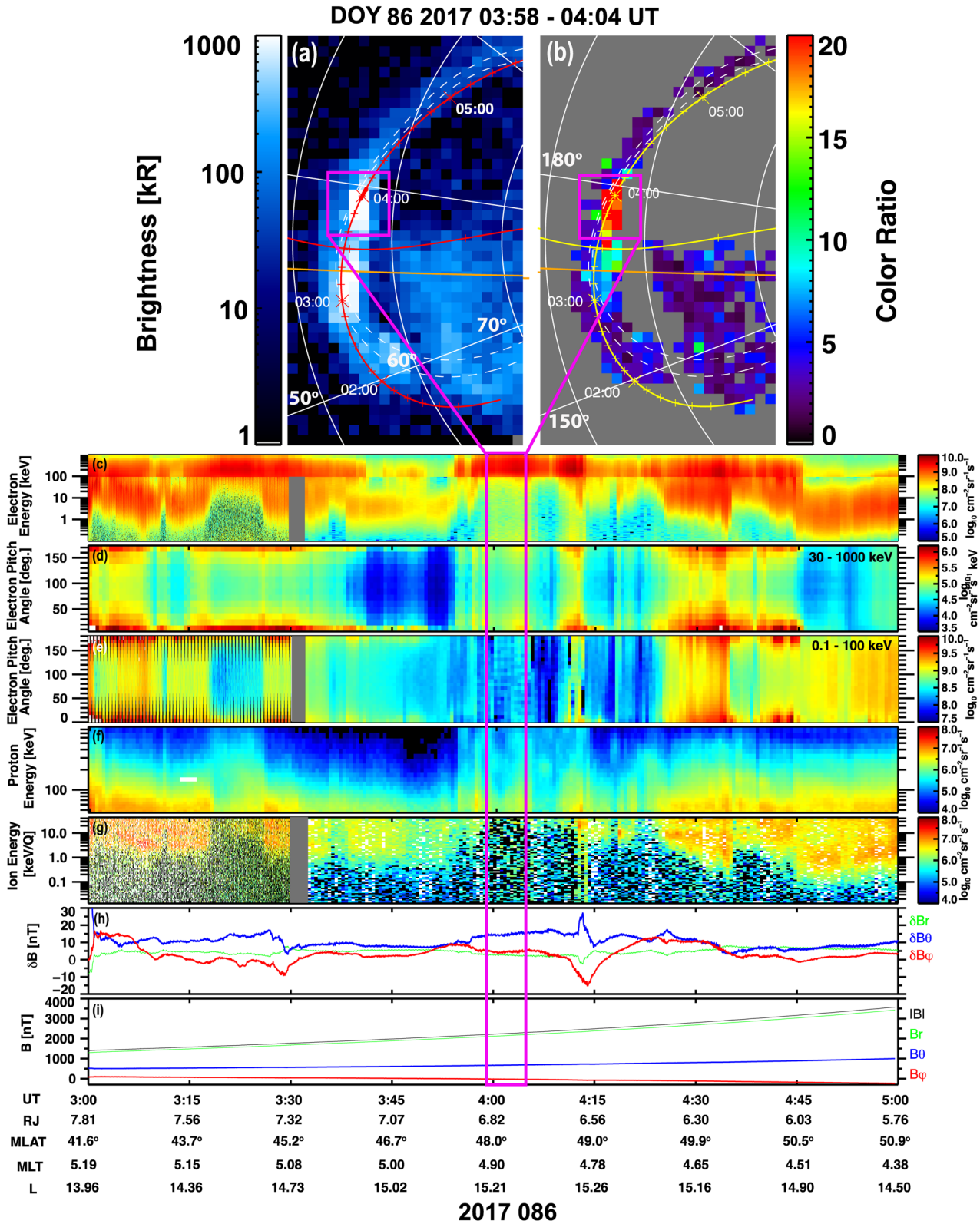


Figure 4.

21699402, 2021, 12, Downloaded from https://agupubs.onlinelibrary.wiley.com/doi/10.1029/2021JA029679 by Portail BibCNRS INSU, Wiley Online Library on [09/12/2022]. See the Terms and Conditions (https://onlinelibrary.wiley.com/terms-and-conditions) on Wiley Online Library for rules of use; OA articles are governed by the applicable Creative Commons License

21699402, 2021, 12, Downloaded from https://agupubs.onlinelibrary.wiley.com/doi/10.1029/2021JA029679 by Portail BibCNRS INSU, Wiley Online Library on [09/12/2022]. See the Terms and Conditions (https://onlinelibrary.wiley.com/terms-and-conditions) on Wiley Online Library for rules of use; OA articles are governed by the applicable Creative Commons License

similar times as the low-energy electrons. At times, the bulk of the ion distributions are at energies above 50 keV. The pitch angle distributions for the protons in Figure 4f (not shown) provide evidence for field-aligned, downgoing beams between ~03:20–03:30 and 04:12–04:14 UT.

Figures 4h and 4i show magnetic field perturbations and magnitudes, respectively, for the radial (B_r), meridional (B_θ), and azimuthal (B_φ) components of Jupiter's magnetic field in a spherical coordinate system. The magnetic field perturbations are calculated by taking the 1 s magnetic field observations and subtracting the ambient field predicted by JRM09 (Connerney et al., 2018) with the latest Jupiter magnetodisc model (Connerney et al., 2020). During this time frame, MAG was operating in a range which corresponds to a quantization step size of 0.128 nT, indicating that the perturbations recorded here (max ~ 27 nT) are well resolved. The periods with the largest perturbations occur at ~03:28–03:30 UT and ~04:13–04:15 UT. Based on the perturbations in B_φ and assuming that all large-scale perturbations are associated with a source region, it seems like Juno first crossed a downward field-aligned current region (decreasing δB_φ) followed by an upward field-aligned current region (increasing δB_φ) in both periods mentioned above. The magnetic field magnitude during this interval ranged from ~1,500 to ~3,700 nT. The maximum perturbations recorded here are up to ~0.7% of the ambient field.

Figure 5 displays the plasma wave electric and magnetic spectral density for the time range shown in Figure 4. The electric field frequencies ranged from ~50 to 200,000 Hz and the magnetic field frequencies from 50 to 20,000 Hz. The emissions just above the electron cyclotron frequency (f_{ce}) (white line) in the top panel are broadband kilometric radio emissions (bKOM). The bKOM is a free-space mode wave generated by the cyclotron maser instability (CMI) at frequencies above f_{ce}. The bKOM appear to be more intense when electrons having keV energies are present. Multi-instrument studies with JADE and Waves when Juno crossed hectometric (HOM) radio sources show that 5–10 keV electrons are able to produce this radiation via CMI (e.g., Louarn et al., 2017, 2018). Studies of non-Io-related decametric (non-Io-DAM) emissions estimated the energy of resonant electrons to be in the range of several keV (Imai et al., 2017). Analogous to HOM and non-Io-DAM radiation, the bKOM resonant energy may also be several keV, which is consistent with the enhanced electron energy observations in Figure 4. More details of these emissions during PJ5 can be found in Imai et al. (2019).

The emission below the f_{ce} is whistler mode auroral hiss with the bulk of the wave energy below 1 kHz. These waves typically propagate along magnetic field lines. Intensification near 03:30 and 04:15 UT correspond to the regions of currents identified in Figure 4h. When their direction of propagation can be determined (between ~03:23 and 03:25 UT), these whistler mode waves appear to be upward propagating and are likely generated at altitudes below the spacecraft. This technique uses orthogonally oriented B and E sensors (as they are on Juno) to measure the phase between signals in these two sensors. This can provide information on whether the propagation is parallel or antiparallel to the magnetic field. Details of this technique can be found in Kolmasova et al. (2018).

Figure 6 combines JADE-E and JEDI observations to examine the differential intensity versus energy distributions, or energy spectra, of 0.1–1,000 keV electrons for selected intervals between 03:00 and 05:00 UT on DOY 86, 2017. We highlight periods where the low-energy electrons are and are not depleted and when the magnetic field perturbations are largest. The electron energy spectra are separated into field-aligned distributions with pitch angles between 0° and 15° (downward-electrons moving toward Jupiter) and between 165° and 180° (upward-electrons moving away from Jupiter). We only select JADE intervals for times when JADE-E has full pitch angle coverage.

Figure 6a shows the energy spectra during a time when the electron intensities peak at ~1–2 keV, have a power-law distribution above those energies, and show little difference between the upward and downward intensities. Figures 6b–6d highlight intervals where the low-energy electron intensities are depleted and the

Figure 4. (a) Ultraviolet (UV) brightness and (b) color ratio images from 03:58 to 04:04 UT on DOY 86, 2017. (c) Energy versus time differential energy flux spectrograms for 0.1–1,000 keV electrons. Electron pitch angle distributions for (d) 30–1,000 keV and (e) 0.1–100 keV electrons, respectively. Electrons with pitch angles of 0° and 180° are moving toward (downward) and away from (upward) Jupiter, respectively. (f) 45–1,000 keV proton and (g) ~0.01–46 keV/q ion differential energy flux spectrograms, respectively. (h) Magnetic field perturbations and (i) magnitudes, respectively. The purple boxes identify the UV emission and color ratio features that Juno is mapping to and the corresponding magnetospheric observations. Data gaps are denoted by gray pixels. Juno's jovicentric distance (R_J), magnetic latitude (MLAT), magnetic local time (MLT), and M-shell (M) are provided.

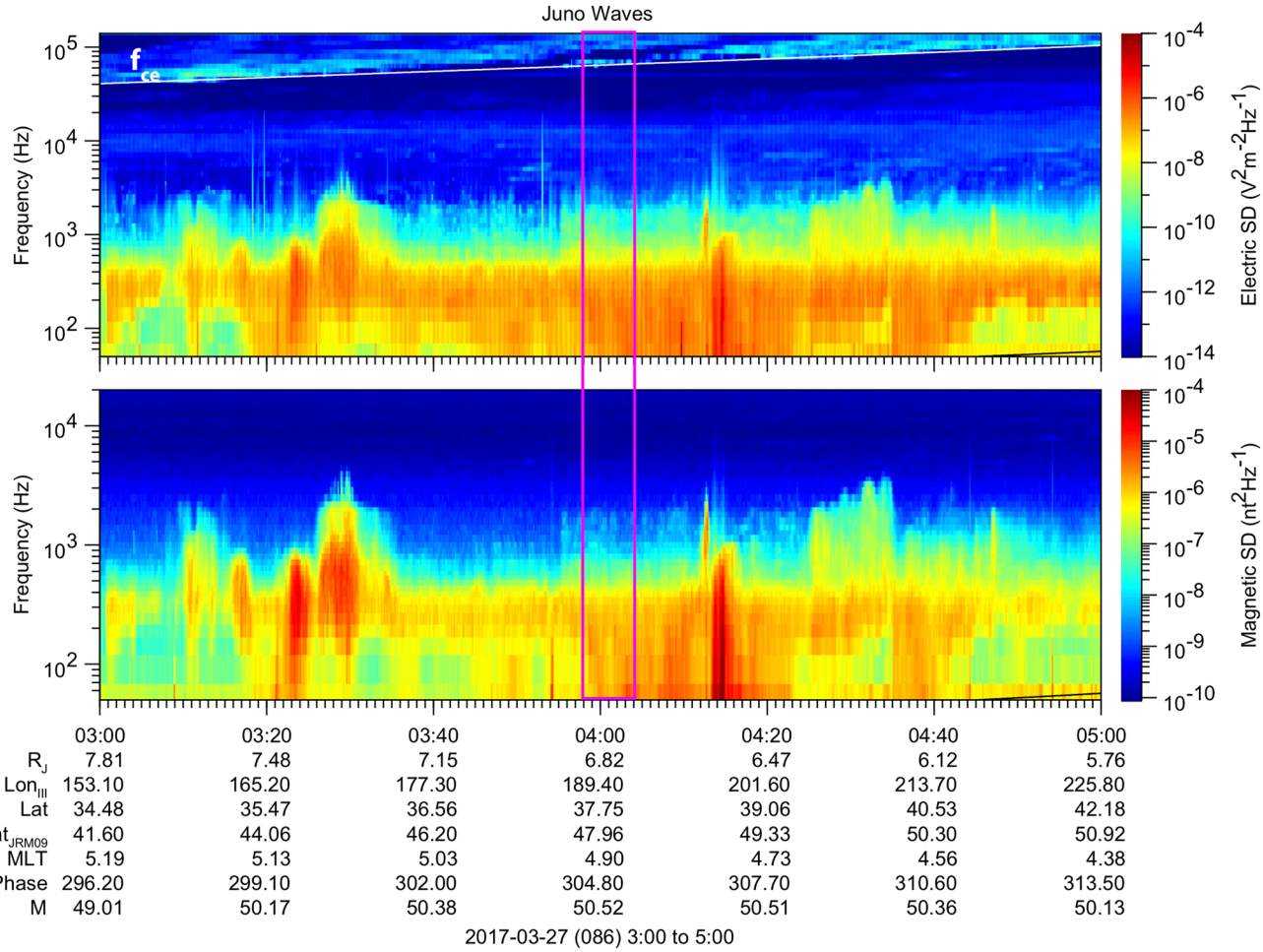


Figure 5. Time series of plasma wave electric (top) and magnetic (bottom) field spectral density from 03:00 to 05:00 UT on day-of-year 86, 2017. The white line in the top panel denotes the electron cyclotron frequency (f_{ce}). Juno's jovicentric distance (R_J), system III longitude (LON_{III}), jovigraphic latitude (Lat), magnetic latitude ($MLat_{JRM09}$), magnetic local time (MLT), phase angle relative to Io, and M-shell (M) are provided. The purple box identifies the same interval as highlighted in Figure 4.

high energy electrons are enhanced. Note the 1–2 order of magnitude increases in the 100–1,000 keV electron intensities compared to Figure 6a. Figure 6c shows energy spectra within the time interval when Juno was mapping to near the dawn storm UV emissions in Figures 4a and 4b. Figure 6d shows energy spectra during the time when Juno observes the largest magnetic field perturbations during this interval, noting the possible upward versus downward intensity asymmetry between 1–50 and 100–1,000 keV. The upward electrons above 100 keV have higher intensities compared to the downward electrons, indicating that further acceleration may be occurring below Juno's altitude.

The scatter in the JADE intensities in Figures 6b and 6c is due to the low-energy plasma being tenuous and variable and the measured signal being at or near the one-count level of the instrument. The JADE and JEDI electron spectra show agreement within up to a factor of 2 at overlapping energies. The intensity increases in the JADE-E spectra between ~20 and 100 keV is likely due to residual background signal not being completely removed from the observations (see Allegrini, Gladstone, et al., 2020 for details). Additional factors may include the different temporal resolution for the JADE and JEDI observations presented here and differences in field-of-view and angular resolution between the two instruments as described in Allegrini, Gladstone, et al. (2020). The distinct bump in intensities observed in all plots between ~150 and 500 keV is due to a JEDI artifact where energetic electrons can begin passing completely through the solid-state detectors (SSDs) at ~420 keV, meaning all their energy is not properly captured and instead these particles give false counts around and above about 160 keV. These local peaks can be thought about as the

21699402, 2021, 12, Downloaded from https://agupubs.onlinelibrary.wiley.com/doi/10.1029/2021JA029679 by Portail BibCNRS INSU, Wiley Online Library on [09/12/2022]. See the Terms and Conditions (https://onlinelibrary.wiley.com/terms-and-conditions) on Wiley Online Library for rules of use; OA articles are governed by the applicable Creative Commons License

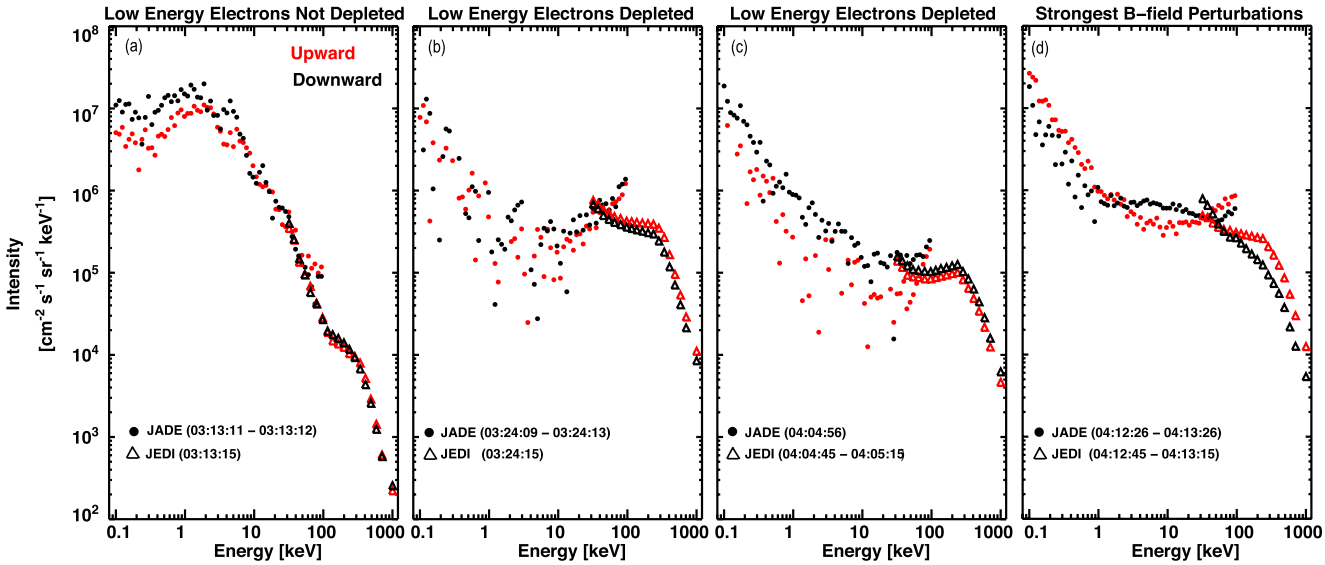


Figure 6. (a–d) Intensity versus energy for 0.1–1,000 keV electrons in Jupiter's polar magnetosphere. Measurements are from the Juno's Jovian Auroral Distributions Experiment Electron (JADE-E) and Jupiter Energetic particle Detector Instruments (JEDIs) on Juno. Black and red symbols represent electron intensities with pitch angles of 0–15° (downward) and 165–180° (upward), respectively. The JADE observations in (a–b) and (c–d) have 1-s and 30-s resolution, respectively, while the JEDI observations have 30-s resolution throughout. The intensities from each instrument are averaged over the time interval specified in each plot.

integrated count rate of electrons above 420 keV that escaped detection of their full energy by JEDI (see Mauk et al., 2017b for details). This feature was partially corrected by redistributing the intensities to their expected energy following the approach outlined in Mauk et al. (2017b).

Table 1 provides estimates for the characteristic energy and energy flux of the electron distributions in Figure 6. Both quantities are calculated using methods described in several recent Juno studies (e.g., Allegrini, Gladstone, et al., 2020; Clark et al., 2018; Mauk et al., 2017a). The characteristic energy reflects the average energy of the electron distributions while the energy flux is a measure of the electron power per unit area. We use JADE observations from 0.1 to 50 keV and JEDI observations from 50 to 1,000 keV in the calculation. The characteristic energy for the upward and downward electron distributions in Figure 6a was 24 and 19 keV, respectively, while their energy flux was 9–10 mW m^{-2}. The characteristic energy and energy flux associated with the distributions in Figures 6b–6d, where the low-energy electrons are depleted and high energy electron intensities are enhanced, were a factor of 5–20 larger. In particular, the downward energy fluxes in these intervals contain significant fraction of the values required to produce the dawn storm UV emissions identified in Figures 2–4, assuming a factor of 10 conversion between energy flux and UV

Table 1
Characteristic Energy and Energy Flux for the Electron Distributions in Figure 6

	Characteristic energy (keV)		Energy flux (mW m^{-2})	
Time interval on DOY 86, 2017 (UT)	Upward	Downward	Upward	Downward
JADE: 03:11:11–03:11:12	24	19	9	10
JEDI: 03:11:15				
JADE: 03:24:09–03:24:13	235	212	179	134
JEDI: 03:24:15				
JADE: 04:04:56	283	247	51	66
JEDI: 04:04:45–04:05:15				
JADE: 04:12:26–04:13:26	221	163	137	69
JEDI: 04:12:45–04:13:15				

21699402, 2021, 12, Downloaded from https://agupubs.onlinelibrary.wiley.com/doi/10.1029/2021JA029679 by Portail BibCNRS INSU, Wiley Online Library on [09/12/2022]. See the Terms and Conditions (https://onlinelibrary.wiley.com/terms-and-conditions) on Wiley Online Library for rules of use; OA articles are governed by the applicable Creative Commons License

21699402, 2021, 12, Downloaded from https://agupubs.onlinelibrary.wiley.com/doi/10.1029/2021JA029679 by Portail BibCNRS INSU, Wiley Online Library on [09/12/2022]. See the Terms and Conditions (https://onlinelibrary.wiley.com/terms-and-conditions) on Wiley Online Library for rules of use; OA articles are governed by the applicable Creative Commons License

brightness (1 mW m^{-2}–10 kR; e.g., Grodent et al., 2001), though we note that neither JADE or JEDI are able to resolve the loss cone at the altitude of these observations.

4. Discussion

We present in situ and remote sensing observations from Juno that connect electrons, ions, magnetic field, and plasma waves in Jupiter's northern polar magnetosphere to transient UV emissions near Jupiter's northern main aurora. The transient UV emissions, consisting of two separate, elongated structures with high color ratios, were observed in the dawn region near the main aurora, extended into the nightside, and rotated to the dayside, suggesting that the generation process of these UV emissions was located in the middle magnetosphere (e.g., Clarke et al., 1998), and moving in the direction of Jupiter's rotation.

These UV emissions have similar characteristics as the UV brightenings described by Gustin et al. (2006) (high color ratios, leading edge traveling in the direction of planetary rotation, trailing edge extending into the nightside), features that are often attributed to dawn storms. According to Bonfond et al. (2021), dawn storms originate near midnight and are initially fixed in magnetic local time. The UV emissions then brighten, their color ratios increasing, as they move toward dawn and are observed to corotate with the planet. Kimura et al. (2017) noted that after onset, dawn storms expand in latitude and longitude, have a rapid increase in total UV power, and produce emissions equatorward of the main auroral oval, during the peak phase of the storm. The UV emissions presented here are consistent with several of these dawn storm features. It was indeed identified as such in Bonfond et al. (2021) and was followed by another dawn storm starting at 07:33 UT on the same day. These dawn storm emissions had a peak UV brightness of at least 1.4 MR and the emissions dimmed as they rotated to Jupiter's dayside. The color ratios show a similar trend, peaking between ∼30 and ∼70 for the leading and trailing emissions, respectively, and reducing significantly as the UV emissions rotated toward the dayside. This suggests that both the energy flux and energy of the electrons producing these emissions were also decreasing. Both the UV brightness and color ratio remained enhanced compared to the surrounding UV emissions for the period examined here.

The electron distributions presented here show several distinct characteristics. At times, the bulk of the electron intensities reside between ∼1 and 100 keV, extend to as low as ∼100–200 eV and are field-aligned. We interpret these observations as plasma sheet electrons with high latitude mirror points. During other times, the electron intensities are depleted at energies below <10 keV, are enhanced at energies of 100s keV, and are also field-aligned. The signature of energetic populations measured simultaneously with depleted lower energies is often associated with the interchange process, whereby flux tube bundles of energized particles (perhaps moving inward and gaining energy by the conservation of the first adiabatic invariant, μ) displace colder plasma in the region. The ions have similar energy distributions as the electrons and at concurrent times. These cold and hot electron and ion populations are interspersed and likely reflect a large-scale dynamic process in Jupiter's equatorial magnetosphere at this time, where ambient plasma in Jupiter's middle magnetosphere is accelerated, heated, and transported to high latitude. For example, Swithenbank-Harris et al. (2021) reported enhanced hot plasma densities at ∼60 R_J, including field-aligned protons and heavy ions, along with reversals of the azimuthal magnetic field, in the equatorial dawn magnetosphere during the dawn storm observed by HST on July 13, 2016. They attribute the heating and acceleration of the equatorial plasma to processes associated with magnetic reconnection and/or disruption of the azimuthal current. Similar processes may be responsible for accelerating the electrons and ions for the dawn storm reported here, prior to them being transported to high latitude.

The characteristic energy and energy flux of the hot electrons reported here are between a factor of 5 and 20 larger than the cold distributions. The characteristic hot downward electron energies of ∼160–250 keV provide further evidence that dawn storms are produced by energetic, 100s of keV, electrons. This is consistent with the high color ratio observations for this event and the long-standing interpretation based on electron energy estimates derived from color ratios of remotely sensed UV emissions from Jupiter's auroral region (e.g., Gustin et al., 2006). The hot electron distributions contain a significant fraction of the energy flux required to produce the UV brightness of at least ∼0.5–1.4 MR for this dawn storm, even at Juno's radial distance of 6–8 R_J, with further enhancements possible closer to the planet. Since neither JADE nor JEDI can resolve the loss cone at the radial distance of these observations, however, we cannot make a definitive

21699402, 2021, 12, Downloaded from https://agupubs.onlinelibrary.wiley.com/doi/10.1029/2021JA029679 by Portail BibCNRS INSU, Wiley Online Library on [09/12/2022]. See the Terms and Conditions (https://onlinelibrary.wiley.com/terms-and-conditions) on Wiley Online Library for rules of use; OA articles are governed by the applicable Creative Commons License

statement about the electron distributions that are precipitating into the atmosphere to produce these dawn storm emissions.

The upward to downward asymmetry in intensity, characteristic energy, and energy flux observed in some of the electron energy spectra presented above indicate that further acceleration is occurring below Juno's altitude during these events. The wave observations during this period suggest that whistler mode auroral hiss and broadband kilometric (bKOM) radio emissions are present at and/or below Juno's altitude. Previous studies have shown whistler mode waves to be associated with electron beams and which could further energize and pitch-angle scatter the electrons (e.g., Elliott et al., 2018; Sulaiman et al., 2020). According to Imai et al. (2019), the intensity of bKOM radio emissions for this northern pass is positively correlated with the UV brightness and color ratio within radio source footprints. These positive correlations imply the existence of particles to wave energy transport (i.e., some of the weakly relativistic electron energy converts into the bKOM wave energy) along the common magnetic field lines between the bKOM radio sources and the UV emissions.

The significant magnetic field perturbations observed at ~03:28–03:30 UT, and especially at ~04:13–04:15 UT, coupled with the field-aligned and bidirectional nature of the electron pitch angle distributions, provide evidence that field-aligned currents are also connected with these events. These perturbations are up to 0.7% of the ambient field at Juno's location, a similar percentage as the magnetic perturbations measured closer to the planet driven by field-aligned currents associated with Jupiter's main aurora (Kotsiaros et al., 2019).

One candidate for producing these auroral emissions is plasma injections (e.g., Mauk et al., 1997), where hot, tenuous plasma is radially transported planetward while cold, dense plasma is transported outward (e.g., Dumont et al., 2014). Plasma injections are thought to be produced by processes related to interchange instability (Mauk et al., 1999; Thorne et al., 1997) and/or tail reconnection (e.g., Gray et al., 2016; Kimura et al., 2017; Krupp et al., 1998; Louarn et al., 2014). Mauk et al. (2002) proposed two mechanisms for how plasma injections can produce auroral emissions at Jupiter. The first is electron scattering by magnetospheric waves that modify the electron pitch angle distribution by scattering electrons into the loss cone. Simulations by Dumont et al. (2018) suggested that electron pitch-angle scattering by whistler mode waves could reproduce the auroral signatures associated with plasma injections. The second mechanism involves a current driven along the pressure gradient between the injected plasma and the surrounding plasma, which must close at the planet. These currents interact with plasma near the planet to produce downward accelerated electrons and auroral emissions that map to the trailing edge of the injected hot plasma distribution that's rotating with Jupiter. The electron distributions associated with the dawn storm emissions studied here were energetic (100s of keV), field-aligned, and bidirectional at Juno's location (6–8 R_J jovicentric distance, 40–50°N magnetic latitude), providing evidence that currents were flowing both toward and away from Jupiter or electrons were accelerated toward Jupiter and mirrored back. These observations are more consistent with the second mechanism being the driver of these emissions, even though these are not necessarily mutually exclusive. The presence of whistler mode auroral hiss at and below Juno's altitude may provide a mechanism for electrons being further energized and scattered into the loss cone as they travel from Juno's location to Jupiter atmosphere.

More recently, Yao et al. (2020) analyzed HST observations of Jupiter's auroral region and found several instances where auroral emissions associated with dawn storms and with injection events were observed at the same time. Examination of in-situ measurements from Juno during one of these intervals revealed evidence of magnetic reconnection in the predawn sector of the equatorial magnetosphere, followed by signatures of magnetic dipolarization a few hours later. The interpretation of these combined observations was that magnetic reconnection and the resulting reconfiguration of the field lines inward of the X-line in the dawn magnetosphere was responsible for the dawn storms and the regions of magnetic dipolarization that corotated with the planet were associated with plasma injections that eventually produced the auroral injection emissions. They suggested a physical connection for these two types of transient auroral emissions with magnetic perturbations being a common feature of both processes. We note that magnetic perturbations were also observed at high latitude during times when Juno was mapping to near the dawn storm studied here, providing further evidence that field line reconfiguration may be associated with these events.

21699402, 2021, 12, Downloaded from https://agupubs.onlinelibrary.wiley.com/doi/10.1029/2021JA029679 by Portail BibCNRS INSU, Wiley Online Library on [09/12/2022]. See the Terms and Conditions (https://onlinelibrary.wiley.com/terms-and-conditions) on Wiley Online Library for rules of use; OA articles are governed by the applicable Creative Commons License

The processes that accelerate the plasma associated with these dawn storms, both in the equatorial magnetosphere and at high latitude near the planet, are not fully understood. The observed electron distributions mapping to the dawn storm emissions that carry the largest energy fluxes are broad in energy, ranging from 1 to 10s of keV up to 1,000 keV, with significant intensity depletions below ~1 keV. Broad energy distributions are often attributed to stochastic particle acceleration (as opposed to acceleration by electrostatic potentials which show a mono-energetic peak in the intensity-energy distributions). Stochastic acceleration appears to be significant in energizing electrons that produce UV emissions associated with Jupiter's diffuse (Li et al., 2017), main (Allegrini et al., 2017; Allegrini Gladstone, et al., 2020; Mauk, Haggerty, et al., 2017; Mauk et al., 2020), polar (Ebert et al., 2017, 2019), and satellite footprint (Allegrini, Mauk, et al., 2020; Szalay et al., 2018, 2020) aurora. Proposed mechanisms include dissipation of turbulent Alfvénic fluctuations (Saur et al., 2003), resonance with whistler mode waves (Elliott et al., 2018; Kurth et al., 2018), electron Landau damping of kinetic Alfvén waves (Saur et al., 2018), incompressible magnetic (Alfvénic) turbulence (Gershman et al., 2019; Sulaiman et al., 2020), and magnetospheric ultralow frequency (1–60 min) Alfvénic waves (Pan et al., 2021). It is recommended that follow-up work focus on whether stochastic or other processes are responsible for accelerating the electrons that produce these dawn storm emissions.

5. Summary and Conclusions

We presented a multi-instrument analysis of a UV dawn storm observed in Jupiter's northern auroral region prior to Juno perijove 5, sampling magnetic field lines at high latitude while remotely observing UV auroral emissions. We combined in situ plasma, energetic particle, magnetic field, and wave observations between 6 and 8 R_J in jovicentric distance and 40°–50°N in magnetic latitude with images of UV brightness and color ratio. The dawn storm UV emissions had brightness up to at least 1.4 MR and high color ratios that indicated a deeper atmospheric penetration depth for the auroral-producing electrons compared to those producing the surrounding UV emissions. Both the brightness and color ratio of these emissions decreased with time as they rotated toward the dayside, indicating that the energy flux and energy of the electrons producing them was also decreasing. The electron distributions were field-aligned, bidirectional and variable in energy, providing evidence for field-aligned currents. The electrons mostly likely producing the dawn storm emissions had broad energy distributions between ~10 and 1,000 keV, significant intensity depletions below 10 keV, characteristic energies from ~160 to 250 keV and downward energy fluxes from ~70 to 130 mW m^{-2} at Juno's altitude. The ion distributions had similar energy distributions at similar times as the electrons, suggesting that they are being accelerated by similar processes. Magnetic perturbations as large as 27 nT, or ~0.7% of the local magnetic field, were observed on field lines that mapped to the dawn storm with variations in B_φ and B_θ providing evidence of upward and downward currents. Whistler mode waves and broadband kilometric radio emissions were also observed.

Based on these observations, we conclude the following:

1. These dawn storm emissions were generated by processes that mapped to Jupiter's nightside and then traveled in the direction of planetary rotation.
2. The high-latitude energetic electron and ion populations measured simultaneously with depleted lower energies are similar to particle observations in the equatorial magnetosphere associated with dynamic processes driven by interchange events, plasma injections, and/or tail reconnection.
3. The electron distributions associated with these dawn storm emissions were field-aligned and had characteristic energies in the 100s of keV range and energies up to at least 1 MeV.
4. The particles were energized prior to arriving at Juno's location, the electron distributions already containing a significant fraction of the energy flux needed to produce the dawn storm UV emissions.
5. The magnetic field perturbations suggestive of upward and downward currents, combined with the field-aligned, bidirectional electrons, indicate that field-aligned currents are associated the processes driving these dawn storm emissions.
6. Whistler mode waves may play a role in enhancing these dawn storm UV emissions while the enhanced broadband kilometric radiation may be a result of one-way energy transport from these dawn storm particles into waves.

Data Availability Statement

The Juno data are available at NASA's Planetary Data System (https://pds.nasa.gov) and the following DOIs. The JADE data used for this study are from data set ID JNO-J/SW-JAD-3-CALIBRATED-V1.0 (doi: 10.17189/1519715), in particular the Version 02 and 03 files from the ion time-of-flight and electron data, respectively. The JEDI data are from data set ID JNO-J-JED-3_CDR-V1.0. The MAG data are from data set ID JNO-J-3-FGM-CAL-V1.0 found at https://doi.org/10.17189/1519711. The Juno Waves data are at https://doi.org/10.17189/1519710. The UVS data are from data set ID JNO-J-UVS-3-RDR-V1.0 which can be found at https://doi.org/10.17189/1518951.

Acknowledgments
This work was supported as a part of the work on the Jovian Auroral Distributions Experiment (JADE) and Juno Ultraviolet Spectrograph (Juno UVS) on NASA's Juno mission. The Jovian Energetic particle Detector Instrument (JEDI) work was funded by NASA's New Frontiers Program for Juno via a subcontract with the Southwest Research Institute. The research at the University of Iowa was supported by the NASA through Contract 699041X with the Southwest Research Institute. This work was supported at the University of Colorado as a part NASA's Juno mission supported by the NASA through contract 699050X with the Southwest Research Institute. The work of MI was supported by the JSPS KAKENHI Grant Number JP20K22371.

References

Allegrini, F., Bagenal, F., Bolton, S., Connerney, J., Clark, G., Ebert, R. W., et al. (2017). Electron beams and loss cones in the auroral regions of Jupiter. *Geophysical Research Letters*, *44*, 7131–7139. https://doi.org/10.1002/2017GL073180

Allegrini, F., Gladstone, G. R., Hue, V., Clark, G., Szalay, J. R., Kurth, W. S., et al. (2020). First report of electron measurements during a Europa footprint tail crossing by Juno. *Geophysical Research Letters*, *47*, e2020GL089732. https://doi.org/10.1029/2020GL089732

Allegrini, F., Mauk, B., Clark, G., Gladstone, G. R., Hue, V., Kurth, W. S., et al. (2020). Energy flux and characteristic energy of electrons over Jupiter's main auroral emission. *Journal of Geophysical Research: Space Physics*, *125*, e2019JA027693. https://doi.org/10.1029/2019JA027693

Ballester, G. E., Clarke, J. T., Trauger, J. T., Harris, W. M., Stapelfeldt, K. R., Crisp, D., et al. (1996). Time-resolved observations of Jupiter's far-ultraviolet aurora. *Science*, *274*(5286), 409–413. https://doi.org/10.1126/science.274.5286.409

Bolton, S. J., Lunine, J., Stevenson, D., Connerney, J. E. P., Levin, S., Owen, T., et al. (2017). The Juno mission. *Space Science Reviews*, *213*(1–4), 5–37. https://doi.org/10.1007/s11214-017-0429-6

Bonfond, B., Grodent, D., Gérard, J.-C., Stallard, T., Clarke, J. T., Yoneda, M., et al. (2012). Auroral evidence of Io's control over the magnetosphere of Jupiter. *Geophysical Research Letters*, *39*, L01105. https://doi.org/10.1029/2011GL050253

Bonfond, B., Yao, Z. H., Gladstone, G. R., Grodent, D., Gérard, J.-C., Matar, J., et al. (2021). Are dawn storms Jupiter's auroral substorms? *AGU Advances*, *2*, e2020AV000275. https://doi.org/10.1029/2020AV000275

Broadfoot, A. L., Belton, M. J. S., Takacs, P. Z., Sandel, B. R., Shemansky, D. E., Holberg, J. B., et al. (1979). Extreme ultraviolet observations from voyager 1 encounter with Jupiter. *Science*, *204*(4396), 979–982. https://doi.org/10.1126/science.204.4396.979

Clark, G., Tao, C., Mauk, B. H., Nichols, J., Saur, J., Bunce, E. J., et al. (2018). Precipitating electron energy flux and characteristic energies in Jupiter's main auroral region as measured by Juno/JEDI. *Journal of Geophysical Research: Space Physics*, *123*, 7554–7567. https://doi.org/10.1029/2018JA025639

Clarke, J. T., Ballester, G., Trauger, J., Ajello, J., Pryor, W., Tobiska, K., et al. (1998). Hubble Space Telescope imaging of Jupiter's UV aurora during the Galileo orbiter mission. *Journal of Geophysical Research*, *103*(E9), 20217–20236. https://doi.org/10.1029/98JE01130

Connerney, J. E. P., Acuna, M. H., & Ness, N. F. (1981). Modeling the Jovian current sheet and inner magnetosphere. *Journal of Geophysical Research*, *86*, 8370–8384. https://doi.org/10.1029/JA086iA10p08370

Connerney, J. E. P., Adriani, A., Allegrini, F., Bagenal, F., Bolton, S. J., Bonfond, B., et al. (2017). Jupiter's magnetosphere and aurorae observed by the Juno spacecraft during its first polar orbits. *Science*, *356*(6340), 826–832. https://doi.org/10.1126/science.aam5928

Connerney, J. E. P., Benn, M., Bjarno, J. B., Denver, T., Espley, J., Jorgensen, J. L., et al. (2017). The Juno magnetic field investigation. *Space Science Reviews*, *213*, 39–138. https://doi.org/10.1007/s11214-017-0334-z

Connerney, J. E. P., Kotsiaros, S., Oliversen, R. J., Espley, J. R., Joergensen, J. L., Joergensen, P. S., et al. (2018). A new model of Jupiter's magnetic field from Juno's first nine orbits. *Geophysical Research Letters*, *45*, 2590–2596. https://doi.org/10.1002/2018GL077312

Connerney, J. E. P., Timmins, S., Herceg, M., & Joergensen, J. L. (2020). A Jovian magnetodisc model for the Juno Era. *Journal of Geophysical Research: Space Physics*, *125*, e2020JA028138. https://doi.org/10.1029/2020JA028138

Dumont, M., Grodent, D., Radioti, A., Bonfond, B., & Gérard, J.-C. (2014). Jupiter's equatorward auroral features: Possible signatures of magnetospheric injections. *Journal of Geophysical Research: Space Physics*, *119*, 10068–10077. https://doi.org/10.1029/2018JA025708

Dumont, M., Grodent, D., Radioti, A., Bonfond, B., Roussos, E., & Paranicas, C. (2018). Evolution of the auroral signatures of Jupiter's magnetosphere injections. *Journal of Geophysical Research: Space Physics*, *123*, 8489–8501. https://doi.org/10.1029/2018JA025708

Ebert, R. W., Allegrini, F., Bagenal, F., Bolton, S. J., Connerney, J. E. P., Clark, G., et al. (2017). Spatial distribution and properties of 0.1–100 keV electrons in Jupiter's polar aurora region. *Geophysical Research Letters*, *44*, 9199–9207. https://doi.org/10.1002/2017GL075106

Ebert, R. W., Greathouse, T. K., Clark, G., Allegrini, F., Bagenal, F., Bolton, S. J., et al. (2019). Comparing electron energetics and UV brightness in Jupiter's northern polar auroral region prior for Juno perijove 5. *Geophysical Research Letters*, *46*, 19–27. https://doi.org/10.1029/2018GL081129

Elliott, S. S., Gurnett, D. A., Kurth, W. S., Mauk, B. H., Ebert, R. W., Clark, G., et al. (2018). The acceleration of electrons to high energies over the Jovian polar cap via whistler mode wave-particle interactions. *Journal of Geophysical Research: Space Physics*, *123*, 7523–7533. https://doi.org/10.1029/2018JA025797

Gérard, J.-C., Bonfond, B., Grodent, D., Radiotti, A., Clarke, J. T., Gladstone, G. R., et al. (2014). Mapping the electron energy in Jupiter's aurora: Hubble Spectral Observations. *Journal of Geophysical Research: Space Physics*, *119*, 9072–9088. https://doi.org/10.1002/2014JA020514

Gérard, J.-C., Bonfond, B., Mauk, B., Gladstone, G. R., Yao, Z. H., Greathouse, T. K., et al. (2019). Contemporaneous observations of Jovian energetic auroral electrons and ultraviolet emissions by the Juno spacecraft. *Journal of Geophysical Research: Space Physics*, *124*, 8298–8317. https://doi.org/10.1029/2019JA026862

Gérard, J.-C., Grodent, D., Dols, V., Prangé, R., Waite, J. H., Gladstone, G. R., et al. (1994). A remarkable auroral event on Jupiter observed in the ultraviolet with the Hubble Space Telescope. *Science*, *266*, 1675–1678. https://doi.org/10.1126/science.266.5191.1675

Gérard, J.-C., & Singh, V. (1982). A model of energy deposition of energetic electrons and EUV emission in the Jovian and Saturnian atmospheres and implications. *Journal of Geophysical Research*, *87*(A6), 4524–4532. https://doi.org/10.1029/JA087iA06p04525

Gershman, D. J., Connerney, J. E. P., Kotsiaros, S., DiBraccio, G. A., Martos, Y. M., Viñas, F. A., et al. (2019). Alfvénic fluctuations associated with Jupiter's auroral emissions. *Geophysical Research Letters*, *46*, 7157–7165. https://doi.org/10.1029/2019GL082951

Gladstone, G. R., Persyn, S. C., Eterno, J. S., Walther, B. C., Slater, D. C., Davis, M. W., et al. (2017). The ultraviolet spectrograph on NASA's Juno mission. *Space Science Reviews*, *213*, 447–473. https://doi.org/10.1007/s11214-014-0040-z

21699402, 2021, 12, Downloaded from https://agupubs.onlinelibrary.wiley.com/doi/10.1029/2021JA029679 by Portail BibCNRS INSU, Wiley Online Library on [09/12/2022]. See the Terms and Conditions (https://onlinelibrary.wiley.com/terms-and-conditions) on Wiley Online Library for rules of use; OA articles are governed by the applicable Creative Commons License

Gray, R. L., Badman, S. V., Bonfond, B., Kimura, T., Misawa, H., Nichols, J. D., et al. (2016). Auroral evidence of radial transport at Jupiter during January 2014. *Journal of Geophysical Research: Space Physics*, *121*, 9972–9984. https://doi.org/10.1002/2016JA023007

Grodent, D. (2015). A brief review of ultraviolet auroral emissions on giant planets. *Space Science Reviews*, *187*, 23–50. https://doi.org/10.1007/s11214-014-0052-8

Grodent, D., Clarke, J. T., Waite, J. H., Cowley, S. W. H., Gerard, J.-C., & Kim, J. (2003). Jupiter's polar aurora emissions. *Journal of Geophysical Research*, *108*(A10), 1366. https://doi.org/10.1029/2003JA010017

Grodent, D., Waite, J. H., Jr., & Gérard, J.-C. (2001). A self-consistent model of the Jovian auroral thermal structure. *Journal of Geophysical Research*, *106*(A7), 12933–12952. https://doi.org/10.1029/2000JA900129

Gustin, J., Cowley, S. W. H., Gérard, J.-C., Gladstone, G. R., Grodent, D., & Clarke, J. T. (2006). Characteristics of Jovian morning bright FUV aurora form Hubble Space Telescope/space telescope imaging spectrograph imaging and spectral observations. *Journal of Geophysical Research*, *111*, A09220. https://doi.org/10.1029/2006JA011730

Imai, M., Greathouse, T. K., Kurth, W. S., Gladstone, G. R., Louis, C. K., Zarka, P., et al. (2019). Probing Jovian kilometric radio sources tied to the ultraviolet main auroral oval with Juno. *Geophysical Research Letters*, *46*, 571–579. https://doi.org/10.1029/2018GL081227

Imai, M., Kurth, W. S., Hospodarsky, G. B., Bolton, S. J., Connerney, J. E. P., Levin, S. M., et al. (2017). Latitudinal beaming of Jovian decametric radio emissions as viewed from Juno and the Nançay Decameter Array. *Geophysical Research Letters*, *44*, 4455–4462. https://doi.org/10.1002/2016GL072454

Kimura, T., Badman, S. V., Tao, C., Yoshioka, K., Murakami, G., Yamazaki, A., et al. (2015). Transient internally driven aurora at Jupiter discovered by Hisaki and the Hubble Space Telescope. *Geophysical Research Letters*, *42*, 1662–1668. https://doi.org/10.1002/2015GL063272

Kimura, T., Nichols, J. D., Gray, R. L., Tao, C., Murakami, G., Yamazaki, A., et al. (2017). Transient brightening of Jupiter's aurora observed by the Hisaki Satellite and Hubble Space Telescope during approach phase of the Juno spacecraft. *Geophysical Research Letters*, *44*, 4523–4531. https://doi.org/10.1002/2017GL072912

Kolmasova, I., Imai, M., Santolik, O., Kurth, W. S., Hospodarsky, G. B., Gurnett, D. A., et al. (2018). Discovery of rapid whistlers close to Jupiter implying similar lightning rates as on Earth. *Nature Astronomy*, *2*(7), 544–548. https://doi.org/10.1038/s41550-018-0442-z

Kotsiaros, S., Connerney, J. E. P., Clark, G., Allegrini, F., Gladstone, G. R., Kurth, W. S., et al. (2019). Birkeland currents in Jupiter's magnetosphere observed by the polar-orbiting Juno spacecraft. *Nature Astronomy*, *3*, 904–909. https://doi.org/10.1038/s41550-019-0819-7

Krupp, N., Woch, J., Lagg, A., Wilken, B., Livi, S., & Williams, D. J. (1998). Energetic particle bursts in the predawn Jovian magnetotail. *Geophysical Research Letters*, *25*(8), 1249–1252. https://doi.org/10.1029/98GL00863

Kurth, W. S., Hospodarsky, G. B., Kirchner, D. L., Mokrzycki, B. T., Averkamp, T. E., Piker, C. W., et al. (2017). The Juno waves investigation. *Space Science Reviews*, *213*, 347–392. https://doi.org/10.1007/s11214-017-0396-y

Kurth, W. S., Mauk, B. H., Elliott, S. S., Gurnett, D. A., Hospodarsky, G. B., Santolik, O., et al. (2018). Whistler mode waves associated with broadband auroral electron precipitation at Jupiter. *Geophysical Research Letters*, *45*, 9372–9379. https://doi.org/10.1029/2018GL078566

Li, W., Thorne, R. M., Ma, Q., Zhang, X.-J., Gladstone, G. R., Hue, V., et al. (2017). Understanding the origin of Jupiter's diffuse aurora using Juno's first perijove observations. *Geophysical Research Letters*, *44*, 10162–10170. https://doi.org/10.1002/2017GL075545

Louarn, P., Allegrini, F., McComas, D. J., Valek, P. W., Kurth, W. S., André, N., et al. (2017). Generation of the Jovian hectometric radiation: First lessons from Juno. *Geophysical Research Letters*, *44*, 4439–4446. https://doi.org/10.1002/2017GL072923

Louarn, P., Allegrini, F., McComas, D. J., Valek, P. W., Kurth, W. S., André, N., et al. (2018). Observation of electron conics by Juno: Implications for radio generation and acceleration processes. *Geophysical Research Letters*, *45*, 9408–9416. https://doi.org/10.1029/2018GL078973

Louarn, P., Andre, N., Jackman, C., Kasahara, S., Kronberg, E., & Vogt, M. (2014). Magnetic reconnection and associated transient phenomena within the magnetospheres of Jupiter and Saturn. *Space Science Reviews*, *187*, 181–227. https://doi.org/10.1007/s11214-014-0047-5

Mauk, B. H., Clark, G., Gladstone, G. R., Kotsiaros, S., Adriani, A., Allegrini, F., et al. (2020). Energetic particles and acceleration regions over Jupiter's polar cap and main aurora; a broad overview. *Journal of Geophysical Research: Space Physics*, *125*, e2019JA027699. https://doi.org/10.1029/2019JA027699

Mauk, B. H., Clarke, J. T., Grodent, D., Waite, J. H., Jr., Paranicas, C. P., & Williams, D. J. (2002). Transient aurora on Jupiter from injection of magnetospheric electrons. *Nature*, *415*, 1003–1005. https://doi.org/10.1038/4151003a

Mauk, B. H., Haggerty, D. K., Jaskulek, S. E., Schlemm, C. E., Brown, L. E., Cooper, S. A., et al. (2017). The Jupiter energetic particle detector instrument (JEDI) investigation for the Juno mission. *Space Science Reviews*, *213*(1–4), 289–346. https://doi.org/10.1007/s11214-013-0025-3

Mauk, B. H., Haggerty, D. K., Paranicas, C., Clark, G., Kollmann, P., Rymer, A. M., et al. (2017a). Juno observations of energetic charged particles over Jupiter's polar regions: Analysis of mono- and bi-directional electron beams. *Geophysical Research Letters*, *44*, 4410–4418. https://doi.org/10.1002/2016GL072286

Mauk, B. H., Haggerty, D. K., Paranicas, C., Clark, G., Kollmann, P., Rymer, A. M., et al. (2017b). Discrete and broadband electron acceleration generating Jupiter's uniquely powerful aurora. *Nature*, *549*(7670), 66–69. https://doi.org/10.1038/nature23648

Mauk, B. H., Williams, D. J., & McEntire, R. W. (1997). Energy-time dispersed charged particle signatures of dynamic injections in Jupiter's inner magnetosphere. *Geophysical Research Letters*, *24*(23), 2949–2952. https://doi.org/10.1029/97GL03026

Mauk, B. H., Williams, D. J., McEntire, R. W., Khurana, K. K., & Roederer, J. G. (1999). Storm-like dynamics of Jupiter's inner and middle magnetosphere. *Journal of Geophysical Research*, *104*(A10), 22759–22778. https://doi.org/10.1029/1999JA900097

McComas, D. J., Alexander, N., Allegrini, F., Bagenal, F., Beebe, C., Clark, G., et al. (2017). The Jovian auroral distributions experiment (JADE) on the Juno mission to Jupiter. *Space Science Reviews*, *213*, 547–643. https://doi.org/10.1007/s11214-013-9990-9

Pan, D.-X., Yao, Z.-H., Manners, H., Dunn, W., Bonfond, B., Grodent, D., et al. (2021). Ultralow-frequency waves in driving Jovian aurorae revealed by observations from HST and Juno. *Geophysical Research Letters*, *48*, e2020GL091579. https://doi.org/10.1029/2020GL091579

Prangé, R., Zarka, P., Ballester, G. E., Livengood, T. A., Denis, L., Carr, T., et al. (1993). Correlated variations of UV and radio emissions during an outstanding Jovian auroral event. *Journal of Geophysical Research*, *98*(E10), 18779–18791. https://doi.org/10.1029/93JE01802

Radioti, A. D., Grodent, D., Gérard, J. C., Bonfond, B., & Clarke, J. T. (2008). Auroral polar dawn spots: Signatures of internally driven reconnection processes at Jupiter's magnetotail. *Geophysical Research Letters*, *35*, L03104. https://doi.org/10.1029/2007GL032460

Saur, J., Janser, S., Schreiner, A., Clark, G., Mauk, B. H., Kollmann, P., et al. (2018). Wave-particle interaction of Alfvén waves in Jupiter's magnetosphere: Auroral and magnetospheric particle acceleration. *Journal of Geophysical Research: Space Physics*, *123*, 9560–9573. https://doi.org/10.1029/2018JA025948

Saur, J., Pouquet, A., & Matthaeus, W. H. (2003). An acceleration mechanism for the generation of the main auroral oval on Jupiter. *Geophysical Research Letters*, *30*(5), 1260–1319. https://doi.org/10.1029/2002GL015761

Sulaiman, A. H., Hospodarsky, G. B., Elliott, S. S., Kurth, W. S., Gurnett, D. A., Imai, M., et al. (2020). Wave-particle interactions associated with Io's auroral footprint: Evidence of Alfvén, ion cyclotron, and whistler modes, *Geophysical Research Letters*, *47*, e2020GL088432. https://doi.org/10.1029/2020GL088432

21699402, 2021, 12, Downloaded from https://agupubs.onlinelibrary.wiley.com/doi/10.1029/2021JA029679 by Portail BibCNRS INSU, Wiley Online Library on [09/12/2022]. See the Terms and Conditions (https://onlinelibrary.wiley.com/terms-and-conditions) on Wiley Online Library for rules of use; OA articles are governed by the applicable Creative Commons License

Swithenbank-Harris, B. G., Nichols, J. D., Allegrini, F., Bagenal, F., Bonfond, B., Bunce, E. J., et al. (2021). Simultaneous observation of an auroral dawn storm with the Hubble Space Telescope and Juno. *Journal of Geophysical Research: Space Physics*, *126*, e2020JA028717. https://doi.org/10.1029/2020JA028717

Szalay, J. R., Allegrini, F., Bagenal, F., Bolton, S. J., Bonfond, B., Clark, G., et al. (2020). Alfvénic acceleration sustains Ganymede's footprint tail aurora. *Geophysical Research Letters*, *47*, e2019GL086527. https://doi.org/10.1029/2019GL086527

Szalay, J. R., Bonfond, B., Allegrini, F., Bagenal, F., Bolton, S., Clark, G., et al. (2018). In situ observations connected to the Io footprint tail aurora. *Journal of Geophysical Research: Planets*, *123*, 3061–3077. https://doi.org/10.1029/2018JE005752

Thorne, R. M., Armstrong, T. P., Stone, S., Williams, D. J., McEntire, R. W., Bolton, S. J., et al. (1997). Galileo evidence for rapid interchange transport in the Io torus. *Geophysical Research Letters*, *24*(17), 2131–2134. https://doi.org/10.1029/97GL01788

Yao, Z. H., Bonfond, B., Clark, G., Grodent, D., Dunn, W. R., Vogt, M. F., et al. (2020). Reconnection- and dipolarization-driven auroral dawn storms and injections. *Journal of Geophysical Research: Space Physics*, *125*, e2019JA027663. https://doi.org/10.1029/2019JA027663

21699402, 2021, 12, Downloaded from https://agupubs.onlinelibrary.wiley.com/doi/10.1029/2021JA029679 by Portail BibCNRS INSU, Wiley Online Library on [09/12/2022]. See the Terms and Conditions (https://onlinelibrary.wiley.com/terms-and-conditions) on Wiley Online Library for rules of use; OA articles are governed by the applicable Creative Commons License